Two-color magneto-optical trap for metastable helium

A. S. Tychkov,* J. C. J. Koelemeij, T. Jeltes, W. Hogervorst, and W. Vassen
Laser Centre Vrije Universiteit, De Boelelaan 1081, 1081 HV Amsterdam, The Netherlands
(Received 31 October 2003; published 5 May 2004)

We describe a powerful scheme which combines laser cooling on two transitions of metastable helium to obtain a high phase-space density. By running a sequence of a large 1083 nm magneto-optical trap (MOT) and a compressed 389 nm MOT, a density increase of more than one order of magnitude is achieved within 5 ms. After compression, 8×10^8 atoms at a central density of 5×10^{10} cm^{-3} remain, while the temperature of the cloud has been reduced from 1 mK to 0.4 mK. The resulting phase-space density (4.1×10^{-6}) is more than one order of magnitude higher than what we achieved by 1083 nm laser cooling only.

DOI: 10.1103/PhysRevA.69.055401 PACS number(s): 32.80.Pj, 34.50.Fa, 34.50.Rk

In the field of Bose-Einstein condensation (BEC), metastable-state noble gases form an interesting subgroup. At present, BEC has been achieved in spin-polarized metastable helium (He^*) [1,2], while progress is made for metastable neon [3,4]. BEC of metastable helium has led to several novel experiments exploiting the high (19.8 eV) internal energy for efficient and nondestructive detection. For instance, ions produced in Penning-ionizing collisions are used to monitor the birth and decay of the condensate, whereas the metastable atoms themselves are detected with nearly unit detection efficiency after dropping the condensate on a microchannel-plate (MCP) electron multiplier [5,6]. Alongside, cold collisions in He^* were investigated. Photoassociation experiments [7] revealed new details about the long-range part of the $2\,^3S+2\,^3P$ molecular potentials and production of long-lived doubly exited He_2 molecules was recently reported [8]. The success of both experiments mentioned above depends strongly on the ability to reach a high phase-space density in the atomic cloud, for which magnetic trapping and evaporative cooling techniques are traditionally used. This stage of the experiment involves a spin-polarized cloud of atoms, in which Penning losses are suppressed by four orders of magnitude as compared to an unpolarized cloud [1,2,9]. This contrasts the situation in the preceding MOT stage, where the atoms are equally distributed among the different magnetic substates, which leads to a Penning loss-rate constant of order 10^{-10} cm^3/s [10,11]. Moreover, Penning losses are enhanced in the presence of near-resonant 1083 nm light, which is commonly used to drive the $2\,^3S_1 \rightarrow 2\,^3P_2$ laser-cooling transition. The resulting light-assisted collisions lead to typical Penning-ionization rate constants as large as 5×10^{-9} cm^3/s [10] and are difficult to circumvent, since the absence of hyperfine structure in ^{4}He prohibits suppression of light-assisted collisions as done in a dark-SPOT [12]. Therefore, optimization of the MOT for trapping a large number of atoms ($>10^9$) results in a large cloud volume and a relatively low density of about 5×10^9 cm^{-3}. This complicates subsequent magnetic trapping and evaporation for which a high density is desired. The relatively high ($\sim$1 mK) temperature of the atoms in the 1083 nm MOT necessitates an additional optical molasses phase, in order to reduce the temperature sufficiently below the trap depth of a magnetic trap. After a molasses phase, which typically takes 1 ms, the density has decreased by nearly a factor of two [13]. The phase-space density obtained before magnetic trapping remains limited to a few times 10^{-7} when using 1083 nm laser cooling. The initial phase of evaporative cooling therefore proceeds slowly and inefficiently [1,2,13]. Improved starting conditions may provide a higher number of atoms at the BEC threshold. This, for instance, may allow further penetration into the hydrodynamic regime. A second motivation for improving the density in a MOT is the possibility this offers to investigate cold collisions in metastable helium.

In search for a way to overcome the disadvantages of the 1083 nm MOT, we recently tested magneto-optically trapping of He^* at the stronger $2\,^3S_1 \rightarrow 3\,^3P_2$ transition (linewidth $\Gamma/2\pi=1.5$ MHz, saturation intensity $I_0=3.3$ mW/cm^2) at 389 nm [14]. The relevant transitions and energy levels are shown in Fig. 1. In Ref. [14] it was demonstrated that the larger laser-cooling force at 389 nm can result in a much smaller cloud volume than can be obtained at 1083 nm. Meanwhile, the smaller wavelength was shown to strongly decrease the cross section for light-assisted collisions, which makes the 389 nm MOT much more suitable for obtaining high densities. Also, the temperature of the

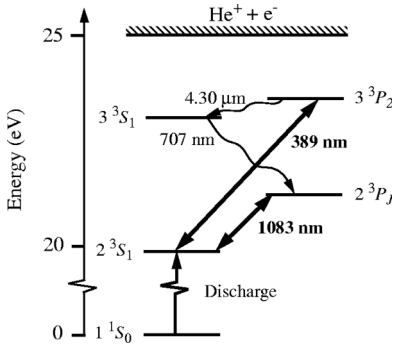

FIG. 1. Helium level scheme. The long-lived $2\,^3S_1$ metastable state is populated in a dc discharge. The $2\,^3S_1 \rightarrow 3\,^3P_2$ (389 nm) and $2\,^3S_1 \rightarrow 2\,^3P_2$ (1083 nm) laser cooling transitions are indicated with bold arrows.

*Electronic address: tychkov@nat.vu.nl

laser-cooled cloud appeared to be lower. Unfortunately, the 389 nm MOT has an intrinsically small loading rate, because its capture velocity is limited by the relatively large Doppler shift. In this paper, we describe the result of an experiment in which we have combined the large loading rate obtained using 1083 nm laser cooling, with the strong compression provided by 389 nm laser cooling.

The experimental setup is based on the He^* apparatus described previously [10,13,15,16]. A liquid-nitrogen cooled dc-discharge source produces a bright beam of He^* atoms, which are subsequently collimated, deflected, and Zeeman decelerated using 1083 nm light. The slow atoms are captured in a 1083 nm MOT at a large detuning $\Delta = -22\Gamma/2\pi = -35$ MHz. A typical steady-state number of trapped atoms $N = 1.2(2) \times 10^9$ is achieved after 0.5 s of loading. The background pressure is about 10^{-9} mbar, and background-collisional losses are negligible compared to the two-body losses which occur at a rate of $10-20\ s^{-1}$. Two-body collisions in the presence of 1083 nm light predominantly result in Penning loss, and the produced positive ions are attracted toward and detected by an MCP. Another MCP is shielded by a grounded grid, such that it detects only neutral metastable atoms. In addition, a charge-coupled-device (CCD) camera is used to record absorption and fluorescence images of the MOT cloud. For the absorption imaging a weak 1083 nm probe beam is used. We have added to the setup six individual 389 nm laser beams, obtained from a frequency-doubled titanium:sapphire laser. The total intensity at 389 nm is typically 200 mW/cm^2 inside the vacuum chamber. This establishes a 389 nm MOT, with a total saturation parameter $S = 60$, spatially overlapped with the 1083 nm MOT. With this beam configuration we were able to run a small, bare 389 nm MOT. Since 10% of the $3\ ^3P_2$ population in this MOT decays via the $3\ ^3S_1$-state cascade which involves visible 707 nm fluorescence (Fig. 1), this MOT is easily viewed using a second CCD camera which monitors 707 nm light only.

With the described setup the following experimental sequence is executed. The 1083 nm MOT is loaded for 1 s. The magnetic field gradient $\partial B/\partial z$ (axial direction) is ramped up from 12 G/cm to 18 G/cm during the last 7.5 ms of the loading phase, allowing sufficient time for the current power supply to respond. Although this increases the density of the cloud and, as a consequence, the two-body loss rate, the duration of the ramp is short enough to ensure that no more than 2% of the atoms are lost. Then, at time $t = 0$ ms, we switch off the 1083 nm light, while simultaneously the 389 nm light is switched on. Using a detuning $\Delta = -10$ MHz (which corresponds to -7Γ), the 389 nm phase lasts for 5–20 ms, after which the cloud is detected by absorption imaging or by time-of-flight (TOF) measurements using the He^*-detecting MCP. During the 389 nm phase, the cloud volume $V = N/n_0$, with n_0 the central density, decreases dramatically within 5 ms. The time dependence of the volume is shown in Fig. 2, with V extracted from absorption images. The time dependences of the rms radii of the cloud in the radial and axial directions of the quadrupole field, σ_ρ and σ_z, fit to an exponential decrease with respective time constants τ_ρ and τ_z. The functional dependence of the radii is of the form $\sigma(t) = \sigma_f - (\sigma_f - \sigma_i)\exp(-t/\tau)$, where σ_i and σ_f are

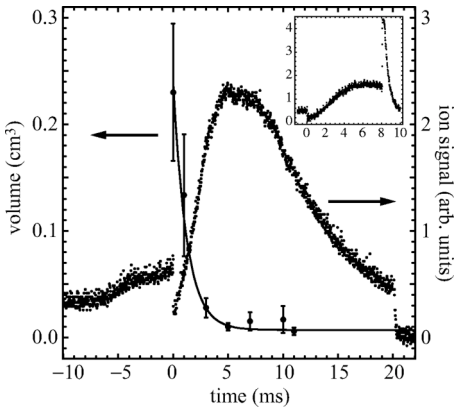

FIG. 2. Ion-detection rate and cloud volume as a function of time. Single data points indicate the volume of the cloud as determined from absorption images during the 389 nm phase, which starts at $t = 0$ ms. The curve represents the volume as obtained from an exponential fit to the cloud-radii data. Error bars indicate primarily shot-to-shot measurement variations. The dotted curve is the typical ion signal during the compression stage. Before $t = 0$ ms, the He^* cloud is contained in a 1083 nm MOT. During the last 7.5 ms of the 1083 nm phase, the magnetic field gradient is increased. At $t = 0$ ms, the 1083 nm light is switched off, and the 389 nm light is switched on. The ion-detection rate rises to a maximum, which corresponds to the maximum density (see text). At $t = 20$ ms the 389 nm MOT is switched off completely, causing the signal to drop to zero. The inset shows the ion signal, when at $t = 8$ ms the 389 nm light is switched off, while simultaneously the 1083 nm light is switched on again.

the initial and final radii. Assuming a Gaussian density distribution, the time dependence of the volume follows from $V(t) = (2\pi)^{3/2}\sigma_\rho^2(t)\sigma_z(t)$. We observe a volume reduction from an initial volume $V_i \sim 0.23(3)\text{cm}^3$, to a final volume $V_f \sim 0.010(3)\text{cm}^3$, with a time constant of 1 ms. This behavior may be not too surprising since the nonequilibrium situation, which is created at $t = 0$ ms when the 389 nm light is switched on, will result in a damped motion of the trapped atoms toward a new steady state. From the absorption images we determine that up to 8×10^8 atoms remain after a 5 ms compression phase, corresponding to an overall transfer efficiency of 70%.

We measured a relatively small capture rate of slow atoms from the He^* beam during the 389 nm phase by running a bare 389 nm MOT under typical conditions. To simplify further analysis, we stop the loading at $t = 0$ ms by switching off the Zeeman-decelerator laser, which does not noticeably affect the number of trapped atoms. The compression leads to a substantial increase in density. Under typical circumstances, a density of $5.0(1.7) \times 10^{10}\ \text{cm}^{-3}$ is observed 4–6 ms after switching to the 389 nm MOT. This number is extracted directly from an absorption image, or indirectly using the number of atoms according to a TOF and a volume measured with an absorption imaging. The TOF signal is calibrated with an absorption image taken after the 1083 nm MOT stage, where the magnetic-field gradients are small, as well as the column density, which ensures reliable calibration. We found a good agreement between the two methods. The achieved high density implies that the 389 nm MOT is

no longer in the temperature-limited regime, where the density distribution of the cloud is governed by the equipartition of the kinetic energy and the potential energy (provided by the MOT trapping lasers only) of the atoms in the MOT [17,18]. Indeed, the volume of the fully compressed cloud is more than two orders of magnitude larger than what one calculates from the spring constants of our 389 nm MOT [19]. This might indicate that radiation trapping forces are at work here, and limit the achievable density. However, also in this respect 389 nm light is advantageous over 1083 nm light: the resonant absorption cross section for 389 nm is almost eight times smaller than for 1083 nm light, whereas the radiative pressure at 389 nm is only 2.7 times larger. Therefore, the outward radiation-trapping force in the cloud is smaller at 389 nm than at 1083 nm.

The relatively small detuning of the 389 nm light also influences the temperature of the cloud. The temperature is determined from the TOF measurements, in which He^* atoms are detected by an MCP after they have been released from the trap. The recorded distribution is fitted to a Maxwell-Boltzmann distribution. Using a detuning of −10 MHz, the temperature of the compressed cloud was about 0.4 mK. This temperature is comparable to what is obtained using a dedicated 1083 nm optical molasses applied to a large, dense He^* cloud [13,15]. Already after 1 ms duration of the 389 nm phase, the TOF distributions correspond well to a Maxwell-Boltzmann distribution at 0.4 mK. Operating at a detuning of −3 MHz resulted in a temperature close to 0.2 mK; however, this also reduces the transfer efficiency considerably. We compared these temperatures with those obtained from the expansion of the cloud using absorption imaging, and agreement to within 20% was found.

The high internal energy of the metastable helium atoms enables us to monitor the dynamics of the compression in real time, making use of the MCP for positive-ion detection. A typical example of the ion signal recorded during a 389 nm compression sequence is shown in Fig. 2 as a dotted curve. As the ions are predominantly produced in light-assisted Penning collisions, the rate of detected ions varies with the density. When the magnetic-field gradient is ramped up during the last 7.5 ms before $t=0$ ms, the density and, therefore, the ion signal increase. At $t=0$ ms, the ion detection rate is seen to fall off abruptly. As the switching to 389 nm takes places too rapidly for the density of the cloud to respond significantly, this proves that two-body Penning collisions in the presence of 389 nm light occur at a considerably smaller rate than in the presence of 1083 nm light. An explanation for this is given in Ref. [14], albeit that in the present case the 389 nm red detuning is much smaller than the 1083 nm red detuning. Still, the loss rate drops by a factor of two when switching to 389 nm. Similarly, a jump in the ion signal is seen when the 389 nm light is switched off and the 1083 nm light is switched on simultaneously (inset Fig. 2). As two-body collisions are dominating the losses in the dense cloud, the ratio of the ion signals just before and after the moment of switching reflects the ratio between the loss rate coefficients for Penning ionization β_{389} and β_{1083}, respectively. We have measured β_{1083} independently, in a similar way as in Ref. [10]. Using this value, we obtain $\beta_{389}=2.9(6)\times10^{-9}$ cm^3/s. The accuracy is set by the determination of β_{1083}, which is limited by the accuracy of the central density determination in the 1083 nm MOT.

TABLE I. Comparison of typical results achieved using a 1083 nm MOT followed by 1083 nm molasses, and by compression in a 389 nm MOT. The temperature after 1083 nm molasses, obtained previously in the same setup, is taken from Ref. [13].

	1083 nm MOT + molasses	1083 nm MOT +389 nm MOT
Number of atoms N	1.1×10^9	5×10^8
Volume V(cm^3)	0.58	0.01
Central density n_0(cm^{-3})	1.7×10^9	5×10^{10}
Temperature T(mK)	0.4[a]	0.4
Phase-space density	1.4×10^{-7}	4.1×10^{-6}

[a]No thermal distribution [13,15].

The shape of the ion signal after $t=0$ ms reflects the strong compression of the cloud, resulting in a steeply increasing signal. Then, when the cloud has attained its final volume and overall losses start to govern the density, the decay of the MOT sets in. Since the number of atoms varies only slowly during the first 5 ms of the compression, the peak in the signal roughly corresponds to the moment at which the maximum density is reached. We checked that the output of the MCP varied linearly with the detection rate during all stages of the experiment. With the 707 nm and 389 nm fluorescence available as a real-time monitor on the total number of trapped atoms, more information on the compression dynamics can in principle be obtained.

The chosen parameters for the 389 nm MOT provide the optimum combination of low temperature, high density, and large number of trapped atoms. The low temperature and high density suggest that the presented scheme offers an alternative to the usual 1083 nm molasses phase before magnetic trapping. However, in a preliminary experiment it was difficult to preserve this high phase-space density during the transfer to our Ioffe-type magnetic trap [13], as a higher bias field and larger gradients are nessesary to build the potential that matches the cloud. On the other hand, the size of the compressed cloud is much smaller than the distance to the trap saddle points. Together with the low temperature this ensures a high transfer efficiency (more than 90% of the atoms for our cloverleaf trap). In addition, 389 nm compression results in a Maxwell-Boltzmann velocity distribution, which is hard to achieve with 1083 nm molasses applied to an optically thick He^* cloud [13,15]. The phase-space density after 389 nm compression is $4.1(1.9)\times10^{-6}$, which is an improvement by more than one order of magnitude as compared to the best result (3×10^{-7}) obtained in our setup by Herschbach *et al.*, using 1083 nm molasses and a 1083 nm MOT [13]. The uncertainty in the value of the phase-space density originates from the uncertainty in the number of atoms and temperature after compression. A comparison between typical results of the two methods, both based on the same 1083 nm MOT, is presented in Table I.

In conclusion, the experimental arrangement presented in this paper increases the phase-space density by more than one order of magnitude as compared to what is achieved

using 1083 nm laser cooling only. With the aim of subsequent magnetic trapping and evaporative cooling toward quantum degeneracy, this is a considerable improvement. Moreover, the achieved low temperature makes the scheme fully exchangeable with 1083 nm molasses. We stress that the described compression scheme is intrinsically superior to compression of a 1083 nm MOT done by increasing the magnetic-field gradient or decreasing the detuning, since the 389 nm wavelength offers smaller two-body losses, a larger cooling force, less radiation trapping, and faster manipulation of the cloud. The performance of the scheme may be further improved by ramping the detuning and magnetic field during the 389 nm phase. In this way a large fraction of the original cloud may be recaptured by the 389 nm MOT, which then can be compressed and cooled down to even smaller volumes and lower temperatures. Finally, it is interesting to note that the described configuration offers possibilities to investigate cold, light-assisted collisions in more detail. The wealth of diagnostic tools opens up many ways to monitor cold atom-atom interactions in the presence of either 1083 nm or 389 nm light, whereas the achieved high density improves the signal-to-noise ratio. Currently, cold-collision phenomena observed in the described setup are subject to further investigation.

We thank P.J.J. Tol for helpful discussions. The Dutch Foundation for Fundamental Research on Matter is gratefully acknowledged for financial support.

[1] A. Robert, O. Sirjean, A. Browaeys, J. Poupard, S. Nowak, D. Boiron, C. I. Westbrook, and A. Aspect, Science **292**, 461 (2001).
[2] F. Pereira Dos Santos, J. Léonard, Junmin Wang, C. J. Barrelet, F. Perales, E. Rasel, C. S. Unnikrishnan, M. Leduc, and C. Cohen-Tannoudji, Phys. Rev. Lett. **86**, 3459 (2001).
[3] S. J. M. Kuppens, J. G. C. Tempelaars, V. P. Mogendorff, B. J. Claessens, H. C. W. Beijerinck, and E. J. D. Vredenbregt, Phys. Rev. A **65**, 023410 (2002).
[4] M. Zinner, P. Spoden, T. Kraemer, G. Birkl, and W. Ertmer, Phys. Rev. A **67**, 010501 (2003).
[5] O. Sirjean, S. Seidelin, J. V. Gomes, D. Boiron, C. I. Westbrook, A. Aspect, and G. V. Shlyapnikov, Phys. Rev. Lett. **89**, 220406 (2002).
[6] S. Seidelin, O. Sirjean, J. V. Gomes, D. Boiron, C. I. Westbrook, and A. Aspect, J. Opt. B: Quantum Semiclassical Opt. **5**, S112 (2003).
[7] N. Herschbach, P. J. J. Tol, W. Vassen, W. Hogervorst, G. Woestenenk, J. W. Thomsen, P. van der Straten, and A. Niehaus, Phys. Rev. Lett. **84**, 1874 (2000).
[8] J. Leonard, M. Walhout, A. P. Mosk, T. Muller, M. Leduc, and C. Cohen-Tannoudji, Phys. Rev. Lett. **91**, 073203 (2003).
[9] P. O. Fedichev, M. W. Reynolds, U. M. Rahmanov, and G. V. Shlyapnikov, Phys. Rev. A **53**, 1447 (1996).
[10] P. J. J. Tol, N. Herschbach, E. A. Hessels, W. Hogervorst, and W. Vassen, Phys. Rev. A **60**, R761 (1999).
[11] N. Herschbach, P. J. J. Tol, W. Hogervorst, and W. Vassen, Phys. Rev. A **61**, 050702 (2000).
[12] M. H. Anderson, W. Petrich, J. R. Ensher, and E. A. Cornell, Phys. Rev. A **50**, R3597 (1994).
[13] N. Herschbach, P. J. J. Tol, A. Tychkov, W. Hogervorst, and W. Vassen, J. Opt. B: Quantum Semiclassical Opt. **5**, S65 (2003).
[14] J. C. J. Koelemeij, R. J. W. Stas, W. Hogervorst, and W. Vassen, Phys. Rev. A **67**, 053406 (2003).
[15] N. Herschbach, Ph.D. thesis, Vrije Universiteit, Amsterdam, 2003.
[16] W. Rooijakkers, W. Hogervorst, and W. Vassen, Opt. Commun. **123**, 321 (1996).
[17] T. Walker, D. Sesko, and C. Wieman, Phys. Rev. Lett. **64**, 408 (1990).
[18] C. G. Townsend, N. H. Edwards, C. J. Cooper, K. P. Zetie, C. J. Foot, A. M. Steane, P. Szriftgiser, H. Perrin, and J. Dalibard, Phys. Rev. A **52**, 1423 (1995).
[19] P. D. Lett, W. D. Phillips, S. L. Rolston, C. E. Tanner, R. N. Watts, and C. I. Westbrook, J. Opt. Soc. Am. B **6**, 2084 (1989).